Electronic Supplementary Information (ESI)

Isovalent cation substitution drives structural transformation and infrared nonlinear optical activity in Eu-based chalcogenides

Ping Feng,‡[a,b,c,d] Sheng-Hua Zhou,‡[b,c,e] Mao-Yin Ran,[b,c] Bingxuan Li,[b,c] Xin-Tao Wu,[b,c] Hua Lin,*[, a,b,c,d] and Qi-Long Zhu*[,a,b,c,d]

[a]*College of Chemistry, Fuzhou University, Fuzhou 350002, China*

[b]*Fujian Science & Technology Innovation Laboratory for Optoelectronic Information of China, Fuzhou 350108, China*

[c]*State Key Laboratory of Structural Chemistry, Fujian Institute of Research on the Structure of Matter, Chinese Academy of Sciences, Fuzhou 350002, China*

[d]*Fujian College, University of Chinese Academy of Sciences, Fuzhou 350002, China*

[e]*Resource environment & Clean energy Laboratory, School of Chemistry and Chemical Engineering, Jiangsu University of Technology, Jiangsu 213001, China*

‡ P. Feng and S. H. Zhou contributed equally to this work.

**E-mail: linhua@fjirsm.ac.cn and qlzhu@fjirsm.ac.cn*

Electronic Supplementary Information (ESI)

Table of Contents

Table S4. The Δd (Å) and $\Delta\theta$ (deg) for the X^{II}-M^{II}-M^{IV}-Q_4 (X^{II} = Eu, Sr, Ba; M^{II} = Zn, Cd, Hg; M^{IV} = Si, Ge, Sn; Q = S, Se) family.

4 References

Electronic Supplementary Information (ESI)

1 Experimental Section

1.1 Materials and Instruments

All reagents used in the present experiments were purchased from commercial sources and directly used without further purification. All weighing processes were completed in an anhydrous and oxygen-free glove box. The semi-quantitative energy dispersive X-ray (EDX, Oxford INCA) spectra were measured with a field emission scanning electron microscope (FESEM, JSM6700F). Powder X-ray diffraction (PXRD) analysis was carried out in a Rigaku Mini-Flex II powder diffractometer (Cu-K_α, λ = 1.5418 Å). UV-vis-NIR absorption measurement was performed in the region of 200−2500 nm at room temperature using an UV-vis-NIR spectrometer (Perkin-Elmer Lambda 950). The reflectance spectrum of the $BaSO_4$ powder was collected as the baseline and the diffuse reflectance data were converted to absorbance internally by the instrument by use of the Kubelka-Munk function.[1] The IR transmittance of the single-crystal sample was measured using the PerkinElmer Spectrum One FT-IR Spectrometer, within the range of 400−4000 cm^{-1}. The thermal stability analyses were measured on a NETZSCH STA 449C simultaneous analyser.

1.2 Synthesis

All reactants were stored and processed in a glove box filled with high-purity argon. To prepare β-$EuZnGeS_4$ crystals, the following materials—Eu_2O_3 powder (4N, Aladdin), Zn powder (4N, Aladdin), Ge powder (5N, Aladdin), S powder (4N, Aladdin), and B powder (4N, Aladdin)—were carefully weighed according to the stoichiometric ratio, resulting in a total mass of 500 mg. Elemental B in the reactive system acts as a reducing agent due to its strong affinity for oxygen. It not only extracts oxygen from metal oxides (e.g., Eu_2O_3) but also helps prevent the detrimental

effects of air, water, and silica tubes on the synthesis process. The powders were then ground, pressed into tablets, and placed in a quartz crucible. The crucible was flame-sealed under a vacuum of 10^{-4} Torr and placed in a computer-controlled muffle furnace. The heating procedure was as follows: the temperature was gradually increased to 1173 K over 50 hours and held at that temperature for 100 hours. Afterward, the furnace was cooled at a rate of 4 K/h, and the tube furnace was shut off once the temperature dropped to 573 K, allowing it to cool naturally to room temperature. The resulting target crystals were red-brown in color and were rinsed with distilled water and ethanol. The synthesized compound retained its weight and color at room temperature for over six months, demonstrating its excellent physical and chemical stability.

1.3 Single-Crystal Structure determination

Taking the high-quality crystal of β-$EuZnGeS_4$ with suitable sizes was selected for single-crystal X-ray diffraction (XRD) analysis. The single-crystal diffraction data collections were collected on a Saturn 724 install with graphite-monochromated Mo-K_α radiation (λ = 0.71073 Å) at room temperature.The absorption correction was performed by the multi-scan method.[2] Using direct methods and maken further refinement by full-matrix least-square fitting on F^2 based on *SHELX−2014* software, the precise struture was determined sussessfully.[3] The atomic coordinates and equivalent isotropic of crystallographic information displacement parameters are given in the Tables S1 and S2. Bond distances (Å) and bond angles (°) of $RbPbPS_4$ are listed in Table S3. CIF of β-$EuZnGeS_4$ has been submitted with CCDC number 2385100.

1.4 Second-Harmonic Generation (SHG) Measurements

The powder SHG property test was investigated by Kurtz-Perry method[4] using a Q-switched laser radiation. The laser radiation at 2900 nm was selected as the laser sources with the laser energy of 10 mJ and $AgGaS_2$ were measured as the benchmark, respectively. Samples of β-$EuZnGeS_4$ and $AgGaS_2$ were ground and sieved into different granule sizes (30−46, 46−74, 74−106, 106−150, and 150−210 μm) for the phase matching measurements. The frequency-doubled output signals were detected via photomultiplier tube and oscilloscope.

1.5 Laser Induced Damage Threshold (LIDT) Measurements

The LIDT of β-$EuZnGeS_4$ at the maximal scope of 150−210 μm was carried out single pulse measurement method[5] and similar scope of $AgGaS_2$ single crystal used to the reference. The whole measuring materials were foist into selfsame plastic holders (thickness: 1 mm and diameter: 8 mm), respectively. Using an optical microscope monitor the exterior change of sample under the 1064 nm laser radiation with pulse width τ_p of 10 ns. Nova II sensor with a PE50-DIF-C energy sensor and a Vernier caliper was used for measuring the power of laser beam and the damage spot radius.

2 Computational Details

The DFT calculations have been performed using the *Vienna ab initio simulation package* (VASP)[6–8] with the Perdew-Burke-Ernzerhof (PBE)[9] exchange correlation functional. The projected augmented wave (PAW)[10] potentials with the valence states 6s, 6p and 4f for Eu, 4s , 4p and 3d for Zn, 4s and 4p for Ge, and 3s and 3p for S, respectively, have been used. A Γ-centered 7×7×5 Monkhorst-Pack grid for the Brillouin zone sampling[11] and a cutoff energy of 750 eV for the plane wave expansion

were found to get convergent lattice parameters. The linear and nonlinear optical calculation was performed in the condition of a Monkhorst-Pack *k*-point mesh of 9×9×7.

The imaginary part of the dielectric function due to direct inter-band transitions is given by the expression:

$$\varepsilon_2(\hbar\omega) = \frac{2e^2\pi}{\Omega\varepsilon_0}\sum_{k,v,c}\left|\left\langle\psi_k^c\left|u\cdot r\right|\psi_k^v\right\rangle\right|^2\delta(E_k^c - E_k^v - E) \quad \ldots\ldots\ldots\ldots (1)$$

where Ω, ω, u, v and c are the unit-cell volume, photon frequencies, the vector defining the polarization of the incident electric field, valence and conduction bands, respectively. The real part of the dielectric function is obtained from ε_2 by a Kramers-Kronig transformation:

$$\varepsilon_1(\omega) = 1 + (\frac{2}{\pi})\int_0^{+\infty} d\omega' \frac{\omega'^2\varepsilon_2(\omega)}{\omega'^2 - \omega^2} \quad \ldots\ldots\ldots\ldots (2)$$

The refractive index $n(\omega)$ can be obtained based on ε_1 and ε_2.

In calculation of the static $\chi^{(2)}$ coefficients, the so-called length-gauge formalism[12] derived by Aversa and Sipe[13] and modified by Rashkeev et al[14] is adopted, which has proven to be successful in calculating the second order susceptibility for semiconductors and insulators. In the static case, the imaginary part of the static second-order optical susceptibility can be expressed as:

$$\chi^{abc} = \frac{e^3}{\hbar^2\Omega}\sum_{nml,k}\frac{r_{nm}^a(r_{ml}^b r_{ln}^c + r_{ml}^c r_{ln}^b)}{2\omega_{nm}\omega_{ml}\omega_{ln}}[\omega_n f_{ml} + \omega_m f_{ln} + \omega_l f_{nm}]$$
$$+ \frac{ie^3}{4\hbar^2\Omega}\sum_{nm,k}\frac{f_{nm}}{\omega_{mn}^2}[r_{nm}^a(r_{mn;c}^b + r_{mn;b}^c) + r_{nm}^b(r_{mn;c}^a + r_{mn;a}^c) + r_{nm}^c(r_{mn;b}^a + r_{mn;a}^b)]$$

……(3)

where r is the position operator, $\hbar\omega_{nm} = \hbar\omega_n - \hbar\omega_m$ is the energy difference for the bands m and n, $f_{mn} = f_m - f_n$ is the difference of the Fermi distribution functions, subscripts a, b, and c are Cartesian indices, and $r^b_{mn;a}$ is the so-called generalized derivative of the coordinate operator in k space,

$$r^b_{nm;a} = \frac{r^a_{nm}\Delta^b_{mn} + r^b_{nm}\Delta^a_{mn}}{\omega_{nm}} + \frac{i}{\omega_{nm}} \times \sum_l (\omega_{lm} r^a_{nl} r^b_{lm} - \omega_{nl} r^b_{nl} r^a_{lm}) \quad \ldots\ldots\ldots\ldots (4)$$

where $\Delta^a_{nm} = (p^a_{nn} - p^a_{mm}) / m$ is the difference between the electronic velocities at the bands n and m.

As the nonlinear optical coefficients is sensitive to the momentum matrix, much finer k-point grid and large amount of empty bands are required to obtain a convergent $\chi^{(2)}$ coefficient. The $\chi^{(2)}$ coefficients here were calculated from PBE wave functions and a scissor operator has been added to correct the conduction band energy (corrected to the experimental gap), which has proven to be reliable in predicting the second order susceptibility for semiconductors and insulators.

Electronic Supplementary Information (ESI)

3 Figures and Tables

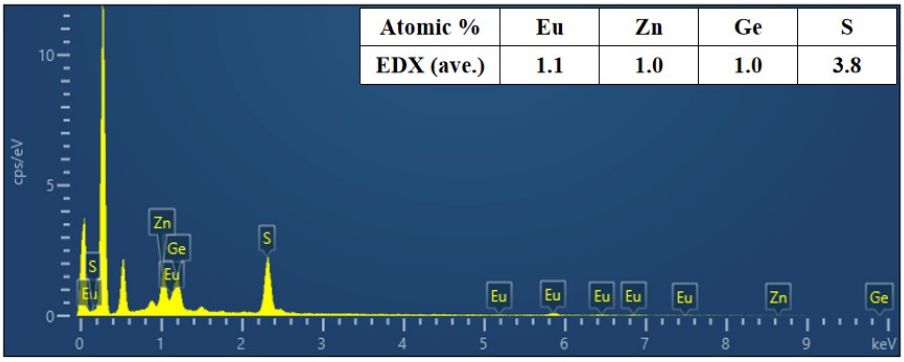

Figure S1. EDX results of β-$EuZnGeS_4$.

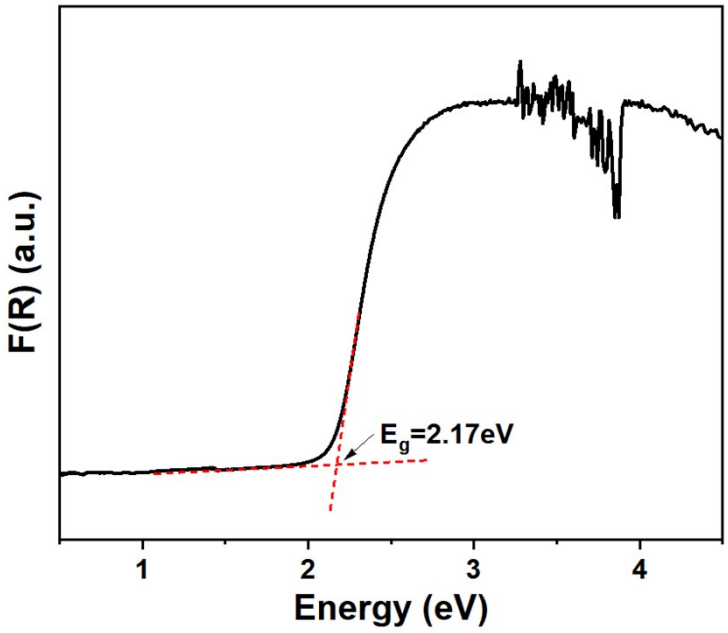

Figure S2. UV−vis−NIR diffuse reflectance spectrum of Eu_2GeS_4.

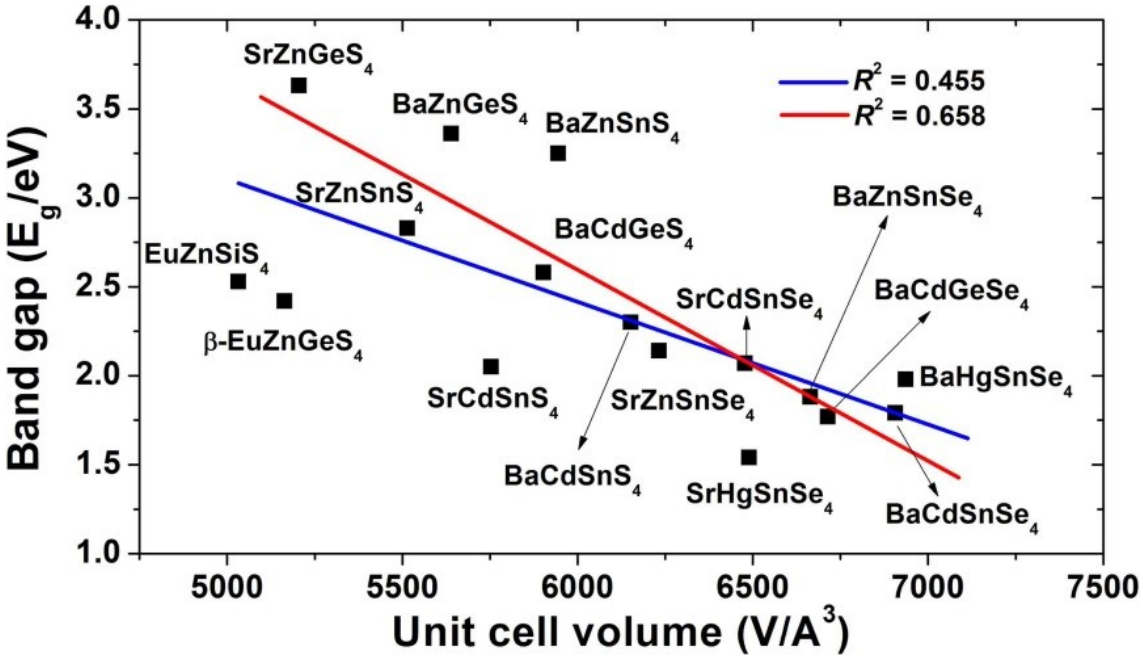

Figure S3. Plot of band gap energies in eV as a function of cell volumes in Å^3 for the members of the X^{II}-M^{II}-M^{IV}-Q_4 family with the space group *Fdd*2.

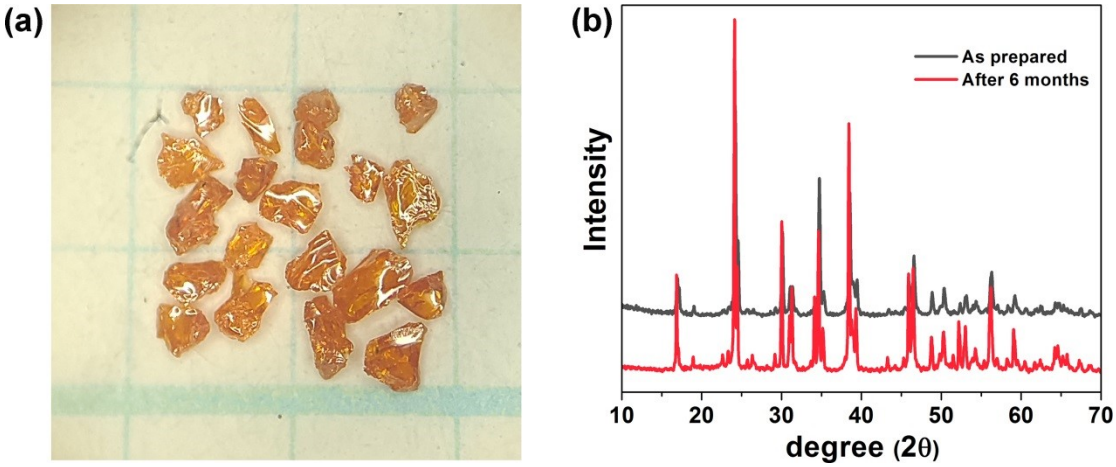

Figure S4. Crystal photo and powder XRD data of the β-$EuZnGeS_4$ compound stored for over 6 months.

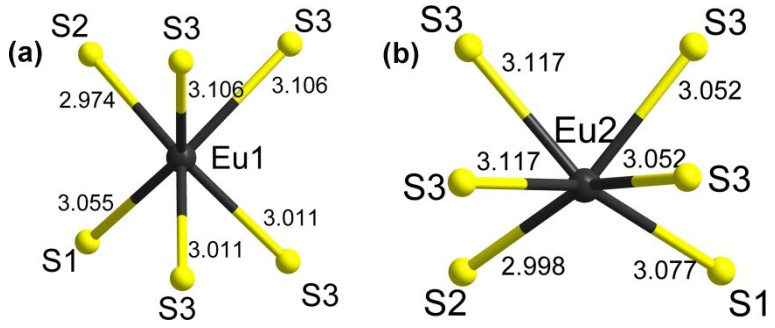

Figure S5. Coordination environment of (a) Eu1 and (b) Eu2 in ternary Eu_2GeS_4.

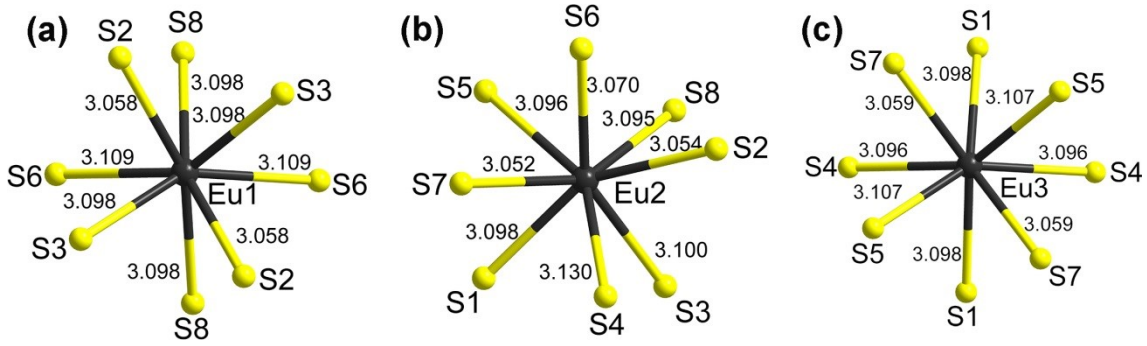

Figure S6. Coordination environment of (a) Eu1, (b) Eu2 and (c) Eu3 in quaternary β-$EuZnGeS_4$.

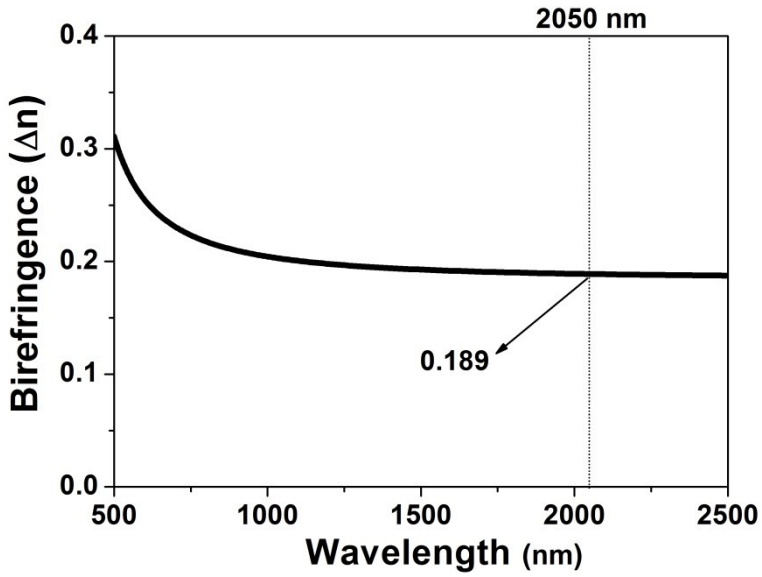

Figure S7. Calculated birefringence (Δn) of β-$EuZnGeS_4$.

Electronic Supplementary Information (ESI)

Table S1. Crystal data and structural refinement details for β-$EuZnGeS_4$.

Empirical formula	β-$EuZnGeS_4$
Formula weight	418.16
Temperature/K	250 (2)
Crystal system	Orthorhombic
Space group	*Fdd*2
a/Å	20.6941(8)
b/Å	20.4059(6)
c/Å	12.2283(4)
α/°	90
β/°	90
γ/°	90
Volume/Å^3	5163.8(3)
Z	32
ρ_{calc} g/cm^3	4.30
μ/mm^{-1}	19.1
Goodness-of-fit on F^2	1.083
Final R indexes [I>=2σ (I)]	R_1 = 0.0187, wR_2 = 0.0450
Final R indexes [all data]	R_1 = 0.0263, wR_2 = 0.0474
Largest diff. peak/hole / e Å^{-3}	0.64/-0.77
Flack parameter	-0.022(13)

[a]: $R_1 = \Sigma||F_o| - |F_c||/\Sigma|F_o|$, $wR_2 = [\Sigma w(F_o^2 - F_c^2)^2/\Sigma w(F_o^2)^2]^{1/2}$

Table S2. Atomic coordinates, equivalent isostropic displacement parameters and bond valence sums (BVS) for of β-$EuZnGeS_4$.

Atom	Wyckff	x	y	z	U_{eq} (Å)[a]	BVS*
Eu1	8a	0.75	0.25	0.89018(12)	0.0109(2)	2.04
Eu2	16b	0.50182(2)	0.24850(4)	0.89260(10)	0.0104(2)	2.06
Eu3	8a	0.75	0.25	0.39447(11)	0.0107(2)	2.04
Zn1	16b	0.62463(9)	0.32375(6)	0.10610(10)	0.0130(3)	1.88
Zn2	16b	0.62585(9)	0.36206(6)	0.63913(11)	0.0125(3)	1.91
Ge1	16b	0.62476(7)	0.38716(5)	0.39133(9)	0.0085(2)	4.00
Ge2	16b	0.62490(8)	0.18157(5)	0.68289(8)	0.0084(3)	4.03
S1	16b	0.6235(2)	0.20508(13)	0.5074(2)	0.0094(6)	2.01
S2	16b	0.6252(2)	0.27880(12)	0.7652(2)	0.0106(6)	2.12
S3	16b	0.70874(18)	0.12891(16)	0.7543(3)	0.0103(8)	2.47
S4	16b	0.70854(19)	0.37987(16)	0.5049(3)	0.0102(8)	1.90
S5	16b	0.54225(19)	0.37912(17)	0.5075(3)	0.0103(8)	1.92
S6	16b	0.54166(18)	0.12869(16)	0.7566(3)	0.0092(8)	1.94
S7	16b	0.6244(2)	0.29685(13)	0.2881(2)	0.0093(6)	2.10
S8	16b	0.6235(2)	0.46787(12)	0.2728(2)	0.0102(6)	2.02

U_{eq} is defined as one third of the trace of the orthogonalized U_{ij} tensor.

*The BVS was calculated by using empirical formula $V_i = \Sigma S_{ij} = \Sigma \exp[(r_0 - r_{ij})/0.37]$, where S_{ij} is the bond valence associated with bond length r_{ij}, and r_0.

Table S3. Selected bond lengths (Å) and angle (°) of β-$EuZnGeS_4$.

Eu1–S2×2	3.058(4)	Zn1–S7	2.292(3)
Eu1–S8×3	3.098(4)	Zn1–S8×2	2.389(3)
Eu1–S3×2	3.098(3)	Zn1–S6×2	2.396(4)
Eu1–S6×2	3.109(3)	Zn1–S3×2	2.407(4)
Eu2–S7×2	3.053(4)	Zn2–S2	2.294(3)
Eu2–S2	3.054(4)	Zn2–S1×2	2.386(3)
Eu2–S6	3.070(3)	Zn2–S5	2.388(4)
Eu2–S8×2	3.095(4)	Zn2–S4	2.399(4)
Eu2–S5×2	3.096(3)	Ge1–S8	2.194(3)
Eu2–S1×2	3.098(4)	Ge1–S4	2.226(4)
Eu2–S3×2	3.100(3)	Ge1–S5	2.227(4)
Eu2–S4×2	3.130(3)	Ge1–S7	2.234(3)
Eu3–S7×2	3.059(4)	Ge2–S1	2.199(3)
Eu3–S4×2	3.096(3)	Ge2–S3	2.220(4)
Eu3–S1×2	3.098(4)	Ge2–S6	2.223(4)
Eu3–S5×2	3.107(3)	Ge2–S2	2.225(2)
∠S2–Eu1–S8×2	66.76(7)	∠S7–Eu3–S4×2	133.51(9)
∠S2–Eu1–S8×2	156.64(5)	∠S7–Eu3–S1×2	64.18(6)
∠S2–Eu1–S3×2	79.13(10)	∠S7–Eu3–S1×2	144.56(5)
∠S2–Eu1–S3×2	69.66(8)	∠S4–Eu3–S1×2	77.67(10)
∠S8–Eu1–S3×2	132.62(9)	∠S4–Eu3–S1×2	79.91(9)
∠S8–Eu1–S3×2	83.38(8)	∠S7–Eu3–S5	76.21(10)
∠S2–Eu1–S6×2	128.70(9)	∠S7–Eu3–S5	77.28(9)

∠S2–Eu1–S6×2	80.35(8)	∠S4–Eu3–S5	68.50(10)
∠S8–Eu1–S6×2	79.06(10)	∠S4–Eu3–S5	146.80(6)
∠S8–Eu1–S6×2	73.16(9)	∠S1–Eu3–S5	76.56(8)
∠S3–Eu1–S6×2	147.46(5)	∠S1–Eu3–S5	135.47(9)
∠S3–Eu1–S6×2	69.40(10)	∠S7–Eu3–S5	77.28(9)
∠S7–Eu2–S2	124.28(10)	∠S7–Eu3–S5	76.21(10)
∠S7–Eu2–S6	76.20(10)	∠S4–Eu3–S5	68.50(10)
∠S2–Eu2–S6	70.14(8)	∠S4–Eu3–S5	146.80(6)
∠S7–Eu2–S8	150.18(8)	∠S1–Eu3–S5	76.56(8)
∠S2–Eu2–S8	66.84(7)	∠S1–Eu3–S5	135.47(9)
∠S6–Eu2–S8	83.92(8)	∠S7–Zn1–S8	101.38(9)
∠S7–Eu2–S5	71.52(8)	∠S7–Zn1–S6	127.34(15)
∠S2–Eu2–S5	130.39(10)	∠S8–Zn1–S6	101.25(14)
∠S6–Eu2–S5	69.83(11)	∠S7–Zn1–S3	127.81(15)
∠S8–Eu2–S5	80.92(10)	∠S8–Zn1–S3	102.35(13)
∠S7–Eu2–S1	64.26(6)	∠S6–Zn1–S3	92.10(9)
∠S2–Eu2–S1	150.36(7)	∠S2–Zn2–S1	100.49(11)
∠S6–Eu2–S1	135.56(10)	∠S2–Zn2–S5	123.81(14)
∠S8–Eu2–S1	121.77(10)	∠S1–Zn2–S5	107.24(13)
∠S5–Eu2–S1	78.75(9)	∠S2–Zn2–S4	125.19(14)
∠S7–Eu2–S3	132.07(10)	∠S1–Zn2–S4	106.87(13)

∠S2–Eu2–S3	80.26(8)	∠S5–Zn2–S4	91.92(11)
∠S6–Eu2–S3	148.38(6)	∠S8–Ge1–S4	118.12(14)
∠S8–Eu2–S3	74.18(9)	∠S8–Ge1–S5	117.88(14)
∠S5–Eu2–S3	126.84(12)	∠S4–Ge1–S5	101.20(12)
∠S1–Eu2–S3	76.02(10)	∠S8–Ge1–S7	104.23(11)
∠S7–Eu2–S4	76.72(9)	∠S4–Ge1–S7	107.45(13)
∠S2–Eu2–S4	78.71(10)	∠S5–Ge1–S7	107.31(13)
∠S6–Eu2–S4	114.64(11)	∠S1–Ge2–S3	119.96(15)
∠S8–Eu2–S4	132.47(10)	∠S1–Ge2–S6	119.42(15)
∠S5–Eu2–S4	145.77(6)	∠S3–Ge2–S6	102.20(10)
∠S1–Eu2–S4	76.21(9)	∠S1–Ge2–S2	104.30(9)
∠S3–Eu2–S4	68.38(11)	∠S3–Ge2–S2	104.59(15)
∠S7–Eu3–S4×2	71.50(8)	∠S6–Ge2–S2	104.56(14)

Table S4. The Δd (Å) and $\Delta\theta$ (deg) for the X^{II}-M^{II}-M^{IV}-Q_4 (X^{II} = Eu, Sr, Ba; M^{II} = Zn, Cd, Hg; M^{IV} = Si, Ge, Sn; Q = S, Se) family.

Number	Compound	Space group	Δd (Å)	$\Delta\theta$ (deg)	Ref.
1	$BaZnSiSe_4$	*Ama*2	0.04	19.49	15
2	$BaZnGeSe_4$	*Ama*2	0.06	19.65	15
3	$SrZnGeS_4$	*Fdd*2	0.07	25.96	16
4	$SrZnSnSe_4$	*Fdd*2	0.07	23.85	17
5	$BaZnSnS_4$	*Fdd*2	0.08	26.02	18
6	$SrZnSnS_4$	*Fdd*2	0.08	26.75	19
7	$BaZnSnSe_4$	*Fdd*2	0.08	23.73	18
8	**β-$EuZnGeS_4$**	***Fdd*2**	**0.077**	**17.15**	**This work**
9	$EuZnSiS_4$	*Fdd*2	0.093	24.92	20
10	$SrCdSnS_4$	*Fdd*2	0.1	28.57	21
11	$SrCdSnSe_4$	*Fdd*2	0.1	25.95	21
12	$BaCdSnSe_4$	*Fdd*2	0.1	24.97	22
13	$BaCdSnS_4$	*Fdd*2	0.1	27.41	23
14	$BaCdGeSe_4$	*Fdd*2	0.11	27.74	24
15	$BaCdGeS_4$	*Fdd*2	0.16	31.34	25
16	$SrHgSnSe_4$	*Fdd*2	0.16	15.9	26
17	$BaHgSnSe_4$	*Fdd*2	0.16	16.8	26
18	$SrCdSiS_4$	*Ama*2	0.13	31.61	27
19	$SrCdGeSe_4$	*Ama*2	0.16	32.3	28
20	$SrCdGeS_4$	*Ama*2	0.17	36.85	28
21	$SrHgGeSe_4$	*Ama*2	0.18	29.27	29

22	$BaHgGeSe_4$	*Ama*2	0.19	28.73	29
23	$SrZnSiSe_4$	*Ama*2	0.22	30.15	30
24	$SrHgSiS_4$	*Ama*2	0.26	45.23	31
25	$SrHgGeS_4$	*Ama*2	0.26	38.27	31
26	$SrHgSnS_4$	*Ama*2	0.28	23.89	26
27	$BaHgSiS_4$	*Ama*2	0.29	46.03	31
28	*β-BaHgSnS*$_4$	*Ama*2	0.3	24.45	26
29	$BaHgGeS_4$	*Ama*2	0.31	38.92	31
30	$EuCdSiS_4$	Ama2	0.1718	44.314	20
31	$EuCdGeS_4$	*Ama*2	0.172	37.11	32
32	$EuCdGeSe_4$	*Ama*2	0.175	32.27	32
33	$EuHgGeSe_4$	*Ama*2	0.221	34.43	33
34	$EuHgGeS_4$	*Ama*2	0.248	38.983	34
35	$EuHgSnS_4$	*Ama*2	0.282	23.87	33
36	α-$BaHgSnS_4$	*Pnn*2	0.27	25.258	35

4 References

1 P. Kubelka and F. Munk, Reflection characteristics of paints, *Z. Techn. Phys.*, 1931, **12**, 593−601.

2. CrystalClear Version 1.3.5 Rigaku Corp.: Woodlands, TX, 1999.

3. P. Kubelka, Ein beitrag zur optik der farbanstriche, *Z. Tech. Phys.*, 1931, **12**, 593–601.

4. S. K. Kurtz and T. T. Perry, A powder technique for the evaluation of nonlinear optical materials, *J. Appl. Phys.*, 1968, **39**, 3798−3813.

5. M. J. Zhang, X. M. Jiang, L. J. Zhou and G. C. Guo, Two phases of Ga_2S_3: promising infrared second-order nonlinear optical materials with very high laser induced damage thresholds, *J. Mater. Chem. C*, 2013, **1**, 4754–4760.

6. G. Kresse, VASP, 5.3.5 http://cms.mpi.univie.ac.at/vasp/vasp/vasp.html.

7. G. Kresse and J. Furthmuller, Efficient iterative schemes for ab initio total-energy calculations using a plane-wave basis set, *Phys. Rev. B: Condens. Matter*, 1996, 11169–11186.

8. G. Kresse and D. Joubert, From ultrasoft pseudopotentials to the projector augmented-wave method, *Phys. Rev. B: Condens. Matter*, 1999, **59**, 1758–1775.

9. Blochl, P. E. Projector augmented-wave method, *Phys. Rev. B: Condens. Matter*, 1994, **50**, 17953–17979.

10 J. P. Perdew, K. Burke and M. Ernzerhof, Generalized gradient approximationmade simple, *Phys. Rev. Lett.*, 1996, **77**, 3865–3868.

11. D. J. Chadi, Special points for Brillouin-zone integrations, *Phys. Rev. B: Condens. Matter*, 1978, **16**, 1746–1747.

12. Z. Fang, J. Lin, R. Liu, P. Liu, Y. Li, X. Huang, K. Ding, L. Ning and Y. Zhang, Computational design of inorganic nonlinear optical crystals based on a genetic algorithm, *CrystEngComm.*, 2014, **16**, 10569–10580.

13. C. Aversa and J. E. Sipe, Nonlinear optical susceptibilities of semiconductors: Results with a length-gauge analysis, *Phys. Rev. B*, 1995, **52**, 14636–14645.

14. S. N. Rashkeev, W. R. L. Lambrecht and B. Segall, Efficient ab initio method for the calculation of frequency-dependent second-order optical response in semiconductors, *Phys. Rev. B*, 1998, **57**, 3905–3919.

15. W. L. Yin, A. K. Iyer, C. Li, J. Y. Yao and A. Mar, Noncentrosymmetric chalcogenides $BaZnSiSe_4$ and $BaZnGeSe_4$ featuring one-dimensional structures, *J. Alloys Compd.*, 2017, **708**, 414.

16. Q. Q. Liu, X. Liu, L. M. Wu and L. Chen, $SrZnGeS_4$: A Dual-Waveband Nonlinear Optical Material with a Transparency Spanning UV/Vis and Far-IR Spectral Regions, *Angew. Chem. Int. Ed.*, 2022, **61**, e202205587.

17. (a) F. Hou, D. Mei, Y. Zhang, F. Liang, J. Wang, J. Lu, Z. Lin and Y. Wu, $SrZnSnSe_4$: A quaternary selenide with large second harmonic generation and birefringence, *J. Alloys Compd.,* 2022, **904**, 163944. (b) X. Pang, R. Q. Wang, X. L. Che and F. Q. Huang, $SrZnSnSe_4$: Synthesis, crystal structure and nonlinear optical properties, *J. Solid State Chem.*, 2021, **297**, 122092.

18. Y. N. Li, Z. X. Chen, W. D. Yao, R. L. Tang and S. P. Guo, Heterovalent cations substitution to design asymmetric chalcogenides with promising nonlinear optical performances, *J. Mater. Chem. C*, 2021, **9**, 8659.

19.Y. L. Zhang, D. J. Mei, Y. Yang, W. Z. Cao, Y. D. Wu, J. Lu and Z. S. Lin, Rational design of a new chalcogenide with good infrared nonlinear optical performance: $SrZnSnS_4$, *J. Mater. Chem. C*, 2019, **7**, 8556.

20. P. Feng, S.-H. Zhou, B.-X. Li, J.-X. Zhang, M.-Y. Ran, X.-T. Wu, H. Lin and Q.-L. Zhu, Realizing Excellent Infrared Nonlinear Optical Performance in Eu-Based Chalcogenides via Rational Cross Substitution Strategy, *ACS Appl. Mater. Interfaces*, 2024, **16**, 52682.

21. Y.-J. Lin, B.-W. Liu, R. Ye, X.-M. Jiang, L.-Q. Yang, H.-Y. Zeng and G.-C. Guo, $SrCdSnQ_4$ (Q = S and Se): infrared nonlinear optical chalcogenides with mixed NLO-active and synergetic distorted motifs, *J. Mater. Chem. C*, 2019, **7**, 4459.

22. K. Wu, X. Su, Z. H. Yang and S. L. Pan, An investigation of new infrared nonlinear optical material: $BaCdSnSe_4$, and three new related centrosymmetric compounds: Ba_2SnSe_4, Mg_2GeSe_4, and $Ba_2Ge_2S_6$, *Dalton Trans.*, 2015, **44**, 19856.

23. N. Zhen, K. Wu, Y. Wang, Q. Li, W. H. Gao, D. W. Hou, Z. H. Yang, H. D. Jiang, Y. J. Dong and S. L. Pan, $BaCdSnS_4$ and $Ba_3CdSn_2S_8$: syntheses, structures, and non-linear optical and photoluminescence properties, *Dalton Trans.*, 2016, **45**, 10681.

24. F. Y. Yuan, C. S. Lin, Y. Z. Huang, H. Zhang, A. Y. Zhou, G. L. Chai and W. D. Cheng, $BaCdGeSe_4$: Synthesis, structure and nonlinear optical properties, *J. Solid State Chem.*, 2021, **302**, 122352.

25. Y.-J. Lin, R. Ye, L.-Q. Yang, X.-M. Jiang, B.-W. Liu, H.-Y. Zeng and G.-C. Guo, $BaMnSnS_4$ and $BaCdGeS_4$: infrared nonlinear optical sulfides containing highly distorted motifs with centers of moderate electronegativity, *Inorg. Chem. Front.*, 2019, **6**, 2365.

26. Y. W. Guo, F. Liang, Z. Li, W. H. Xing, Z. S. Lin, J. Y. Yao, A. Mar and Y. C. Wu, $AHgSnQ_4$ (A = Sr, Ba; Q = S, Se): A Series of Hg-Based Infrared Nonlinear-Optical Materials with Strong Second-Harmonic-Generation Response and Good Phase Matchability, *Inorg. Chem.* 2019, **58**, 10390.

27. H.-D. Yang, M.-Y. Ran, S.-H. Zhou, X.-T. Wu, H. Lin and Q.-L. Zhu, Rational designviadual-site aliovalent substitution leads to an outstanding IR nonlinear optical material with well-balanced comprehensive properties, *Chem. Sci.*, 2022, **13**, 10725.

28. Y. W. Dou, Y. Chen, Z. Li, A. K. Iyer, B. Kang, W. L. Yin, J. Y. Yao and A. Mar, $SrCdGeS_4$ and $SrCdGeSe_4$: Promising Infrared Nonlinear Optical Materials with Congruent-Melting Behavior, *Cryst. Growth Des.*, 2019, **19**, 1206.

29. Y. W. Guo, F. Liang, W. L. Yin, Z. Li, X. Y. Luo, Z. S. Lin, J. Y. Yao, A. Mar and Y. C. Wu, $BaHgGeSe_4$ and $SrHgGeSe_4$: Two New Hg-Based Infrared Nonlinear Optical Materials, *Chem. Mater.*, 2019, **31**, 3034.

30. M. J. Ma, J. H. Dang, Y. D. Wu, X. M. Jiang and D. J. Mei, Optimal Design of Mid-Infrared Nonlinear-Optical Crystals: From $SrZnSnSe_4$ to $SrZnSiSe_4$, *Inorg. Chem.*, 2023, **62**, 6549.

31. X. Zhang, H. Wu, Z. Hu, J. Wang, Y. Wu and H. Yu, $A^{II}HgM^{IV}S_4$ (A^{II} = Sr, Ba, M^{IV} = Si, Ge): A Series of Materials with Large Second Harmonic Generation Response and Wide Band Gaps, *Adv. Optical Mater.*, 2023, **12**, 2301735.

32. W. Xing, N. Wang, Y. Guo, Z. Li, J. Tang, K. Kang, W. Yin, Z. Lin, J. Yao and B. Kang, Two rare-earth-based quaternary chalcogenides $EuCdGeQ_4$ (Q = S, Se) with strong second-harmonic generation, *Dalton Trans.*, 2019, **48**, 17620.

33. W. Xing, C. Tang, N. Wang, C. Li, Z. Li, J. Wu, Z. Lin, J. Yao, W. Yin and B. Kang, $EuHgGeSe_4$ and $EuHgSnS_4$: Two Quaternary Eu-Based Infrared Nonlinear Optical Materials with Strong Second-Harmonic-Generation Responses, *Inorg. Chem.*, 2020, **59**, 18452.

34. M. Yan, Z.-D. Sun, W.-D. Yao, W. Zhou, W. Liu and S.-P. Guo, A highly distorted HgS_4 tetrahedron-induced moderate second-harmonic generation response of $EuHgGeS_4$, *Inorg. Chem. Front.*, 2020, **7**, 2451.

35. C. L. Teske, Preparation and crystal-structure of barium-mercury-thiostannate (IV), $BaHgSnS_4$, *Z. Naturforsch. B*, 1980, **35**, 7.